Astron. Astrophys. 68, 367—379 (1978)

ASTRONOMY AND ASTROPHYSICS

Two-frequency High Resolution Observations of 3C 382 and 3C 386

R. G. Strom[1], A. G. Willis[2]* and A. S. Wilson[2,3]

[1] Netherlands Foundation for Radio Astronomy, Radiosterrenwacht, 7990 AA Dwingeloo, The Netherlands
[2] Sterrewacht, Leiden, The Netherlands
[3] Astronomy Centre, University of Sussex, Falmer, Brighton BN1 9QH, England

Received December 6, 1977

Summary. Aperture synthesis maps of the radio galaxies 3C 382 and 3C 386 have been made at wavelengths of 21 cm and 6 cm. The observations show that each source has double structure on a scale of 3′, and a compact central component which coincides with the optical galaxy.

There is evidence that the flux density of the central component of 3C 382 changed by 25% before 1974, and we suggest that the galaxy may be associated with the X-ray source 4U 1825+33. Both 3C 382 and 3C 386 exhibit strong linear polarization at the two wavelengths, and this has been used to derive the distributions of rotation measure, depolarization and magnetic field direction. These and other parameters are discussed in terms of physical processes and the source environment.

Key words: radio galaxies — polarization — magnetic fields — rotation measure — radio variability

1. Introduction

In order to come to a better understanding of the double radio source phenomenon, and gain insight into the physical processes involved, many studies have been made of individual sources using aperture synthesis techniques at different frequencies. This paper describes observations made with the Westerbork Synthesis Radio Telescope (WSRT) at 21 cm (1415 MHz) and 6 cm (4995 MHz) of the intermediate luminosity radio galaxies 3C 382 and 3C 386. The study was undertaken to improve upon earlier observations with the Cambridge One Mile telescope (Riley and Branson, 1973; Mackay, 1970), from which it was known that both objects would be suitable for WSRT measurement.

The observing and reduction techniques used were standard, and are described elsewhere (Högbom and Brouw, 1974; van Someren Gréve, 1974; Weiler, 1973). Tables 1 and 2 summarize parameters relevant to the present observations. Dynamic range limitations, especially in the 6 cm maps, made it unprofitable to intercompare the 21 and 6 cm total intensity data in detail. We have, however, been able to compare the polarization properties, and to facilitate this have made maps with identical resolution for each source at the two wavelengths with the help of the CLEAN algorithm (Högbom 1974). CLEAN has also been used on all maps presented as contour diagrams.

Send offprint requests to: R. G. Strom

* Now at Department of Physics, Brandeis University, Waltham, Mass. 02154, USA

2. The 3C 382 Observations

The distributions of total intensity (I), linearly polarized intensity ($(Q^2+U^2)^{1/2}$) and percentage linear polarization ($100(Q^2+U^2)^{1/2}/I$) at 6 cm are shown in Figures 1a—c respectively. Figures 2a—c present the 21 cm results in a similar format. A summary of the radio properties, as derived from our data, appears in Table 3.

The total intensity structures are similar to those presented by Riley and Branson (1973) at 6 cm and Macdonald et al. (1968) at 21 cm. 3C 382 is a typical triple, with a high brightness region near the outermost edge of each outer component and a compact source close to the radio centroid. Among the significant morphological details in the I maps are the difference in observed surface brightness between the two outer peaks (nearly a factor of two), the fact that the peak of the southwestern component is set well behind the "leading edge" and the shape of the low brightness "tails" trailing away from the outer components. The non-alignment of the tails (i.e. the angle between the tail extension and the source axis, defined as a line drawn between the high brightness peaks in the outer components) is much larger in 3C 382 than is typical in this class of object (Harris, 1974). Further, the ridge line of the northeast component has a noticeable wiggle, extending first southwest from the outer hot spot (in the direction of the highest peak of the southwestern lobe), then almost due west, and veering southwest again to join the central component. In contrast, the ridge line of the tail of the southwest component does not join the central

Table 1. Observing Log for 3C 382 and 3C 386

Field	Wavelength	Field Center	Shortest spacing, increment	Time	Date
3C 382	6 cm	$18^h33^m12^s$, 32°39′22″	54 m, 72 m	1×12^h	1974.3
3C 382	21	$18^h33^m12^s$, 32°39′22″	72 m, 72 m	1×12^h	1974.5
3C 386	6	$18^h36^m12^s$, 17°9′6″	54 m, 36 m	2×12^h	1974.3
3C 386	21	$18^h36^m12^s$, 17°9′6″	72 m, 72 m	1×12^h	1974.5

Table 2. Map Parameters for 3C 382 and 3C 386

	3C 382		3C 386	
Wavelength (cm)	6	21	6	21
Primary beam half power width (arc min)	11	37	11	37
Synthesized beam half power width, $\alpha\times\delta$ (arc sec)	7×13	23×43	7×23	23×78
Distance between grating responses, $\alpha\times\delta$ (arc min)	3×6	10×19	6×20	10×34

Table 3. Observed Radio Properties of 3C 382

	East Lobe	West Lobe	Total
Angular size, major × minor axis	76″ × 41″	97″ × 35″	184″ × 101″
Position angle, major axis	70°	110°	50°
Flux density, 21 cm	3.3 Jy[a]	2.2 Jy	5.5 Jy
Flux density, 6 cm	1.5 Jy[a]	1.1 Jy	2.6 Jy
Spectral index, α_{21}^{6}	−0.61	−0.56	−0.59
Degree of polarization, 21 cm	0.8%	5.4%	2.0%
Polarization p.a., 21 cm	99°	37°	43°
Degree of polarization, 6 cm	2.5%	5.3%	1.3%
Polarization p.a., 6 cm	7°	80°	60°

[a] Includes the flux of the central component, which is 0.175±0.005 Jy at 6 cm and 0.15±0.07 Jy at 21 cm.

source at all, but trails off east and south of the outer peak. It is also of interest to note that the nuclear source itself is displaced by about 15″ from the source axis.

More pronounced distortions of double structure—ranging from "bent" sources like 3C 465 to "head-tail" radio galaxies like 3C 129—have been ascribed to motion of the galaxy through an intracluster medium. It is thus interesting to note that the $14^m.5$ optical galaxy ($z=0.0578$; Schmidt, 1965) associated with 3C 382 is, according to Zwicky and Herzog (1963), a member of the "medium compact, near" cluster Zw 1831.2+3154 which has 118 members. However, there is also a strong dependence of radio galaxy morphology on luminosity (Fanaroff and Riley, 1974; Gavazzi and Perola, 1977), in the sense that radio galaxies with luminosity $\leqq 2\ 10^{25}$ W Hz^{-1} at 178 MHz (roughly the luminosity of 3C 382) exhibit a wide variety of structures whose possible causal relationship to the circumgalactic environment remains uncertain.

Figure 3 shows the 6 cm map of 3C 382 superimposed on a copy of the Palomar Sky Survey "red" print. It is clear that the major axis of the associated optical galaxy lies along position angle $\simeq 90°$ and thus that its orientation does not bear any simple relation to the axis of the radio source. The plate also shows that another member of the cluster Zw 1831.2+3154, with magnitude comparable to that of the radio galaxy, lies, in projection, just to the south of the radio hot spot in the eastern component of 3C 382 (see also Adams, 1977).

The major difference between the total intensity emission at 6 cm and 21 cm, after allowing for the difference in resolution, is the increase in the relative strength of the central nuclear source at the shorter wavelength. Although Riley and Branson (1973) also find a flat spectrum for this component ($\alpha^1=0.0\pm0.2$), the 6 cm flux density they measure (230±20 mJy) is greater than ours (175±5 mJy). This difference cannot be the result of different flux density scales as both observations were calibrated assuming a flux density of 8.2 Jy for 3C 147. Moreover, the strength of the compact hot spot in the northeastern lobe is close to that measured by Riley and Branson with similar resolution. The flux density of the central source has, therefore, decreased by some 25% between the summer of 1972 and March 1974 (the Cambridge observations were made

[1] Where α is defined by the relationship, flux density $\propto$ frequency$^{\alpha}$

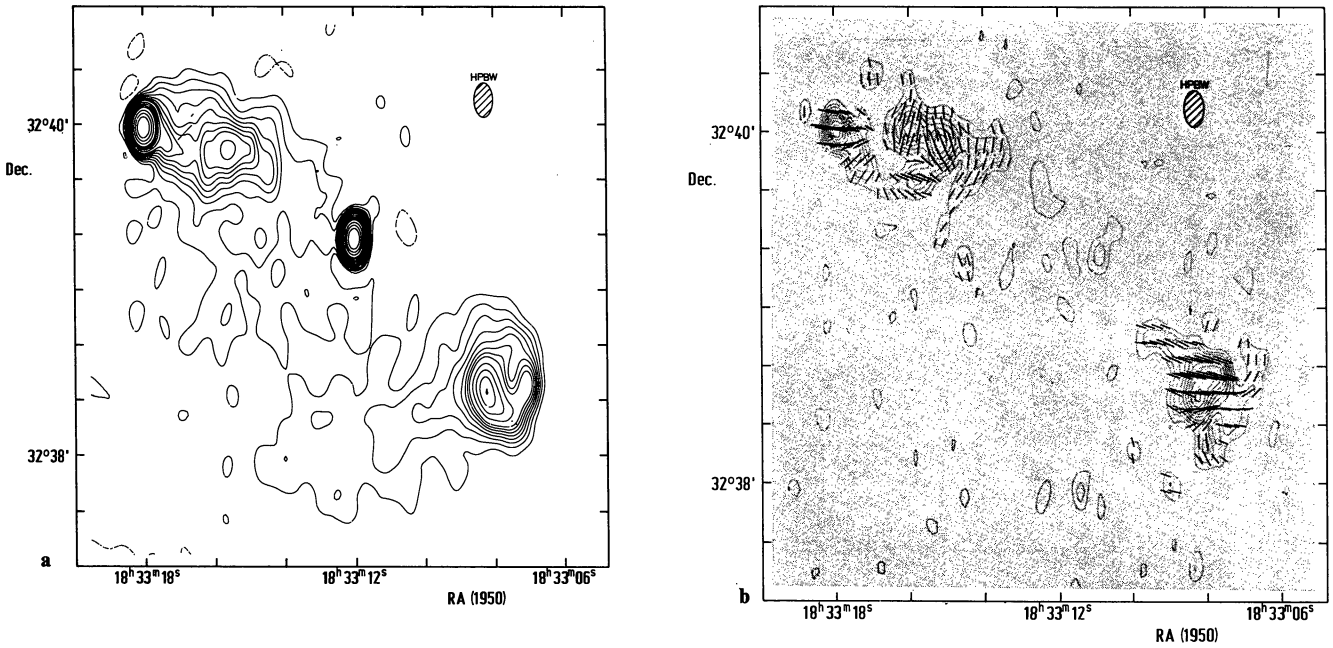

Fig. 1. Maps of 3C 382 made at a wavelength of 6 cm. **a** The total intensity distribution, shown with contour values of −5 (dashed), 5, 10, 15, 20, 25, 30, 35, 40, 50, 60, 70, 80, 100, 120 and 140 mJy/beam. **b** The linearly polarized intensity distribution (contours) and position angles of the electric vectors (lines). The contour values are, 3, 4.5, 6, 7.5, 9, 10.5, 12, 13.5, and 15 mJy/beam. **c** Contours showing the degree of linear polarization (with values indicated in per cent) superimposed on the total intensity contours

between May and August 1972; Riley, private communication).

The polarization structure of 3C 382 (Figs. 1b and 2b) is more complex than the total intensity distribution, especially at 6 cm. In general, however, the position angles vary slowly. Figure 4a shows the difference between the 21 cm and 6 cm position angles (in the sense PA(21 cm)−PA(6 cm)) obtained from maps with the same resolution. Of course it is impossible to derive the rotation measure (*RM*) unambiguously from data at only two wavelengths. We have, therefore, examined our integrated values (Table 3) and a 73 cm measurement (Conway et al., 1972) as well as some limited 2 cm data (J. R. Baker, private communication) and find the measurements to be consistent with an integrated *RM* $= +68$ rad m^{-2}. It must be emphasized that this value should be regarded as very provisional in view of the few wavelengths at which polarization has been measured. However, guided by it, the change in the position angle of the electric vector between 6 cm and 21 cm at individual points in the source (Fig. 4a) may be converted into a distribution of *RM*. These values of *RM* were then used to derive the configuration of the magnetic field projected onto a plane perpendicular to the line of sight (Fig. 5) by extrapolating the position angles to zero wavelength. Also shown, in Figure 4b, is the distribution of depolarization ($=100\times$(21 cm degree of polarization)/(6 cm degree of polarization)).

It is clear from Figure 5 that the magnetic field has orthogonal directions in different regions, not only on the scale of the whole source but also within the eastern component. This fact, coupled with the variation of *RM* over the source as a whole and within the eastern component, presumably accounts for: a) The low percentage polarization of the integrated emission from the eastern component and from the source as a whole at both 6 cm and 21 cm (Table 3), despite the much higher percentages found on the maps (Figs. 1c and 2c); b) The large

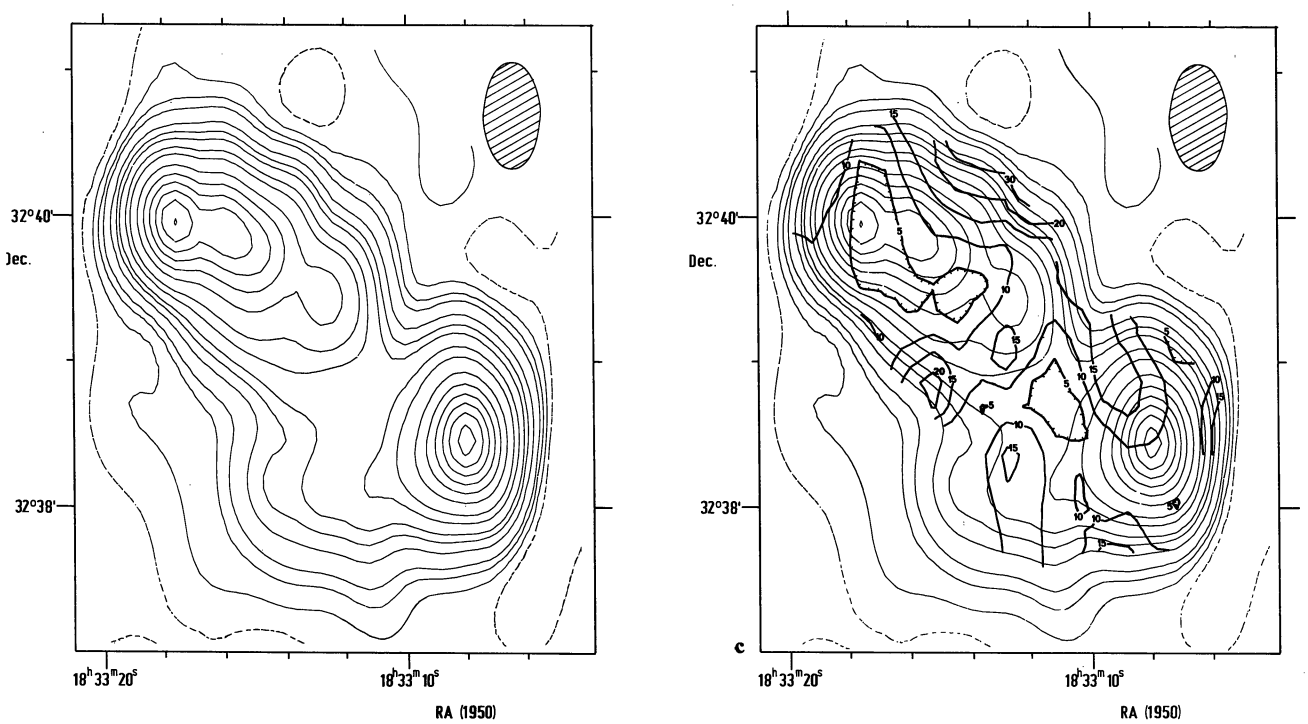

Fig. 2. Maps of 3C 382 made at 21 cm. **a** Contours showing the total intensity distribution with values of −5 (dashed), 5, 15, 25, 50, 75, 100, 150, 200, 300, 400, 500, 600, 700 and 800 mJy/beam. **b** Contours of linearly polarized intensity and lines showing the position angle distribution. Contour values are, 5, 15, 25, 37.5, 50, 67.5, and 75 mJy/beam. **c** Contours of the degree of linear polarization superimposed on total intensity contours

decrease in the percentage polarization of the integrated emission of the eastern component between 6 cm and 21 cm (Table 3), in spite of the relative lack of depolarization in this component apparent in Figure 4b. (Note that the anomalous depolarization observed near the central component in Figure 4b may be ascribed to its differing spectral index from the surrounding, extended emission; the central component is essentially unpolarized, $\lesssim 1\%$ at 6 cm); c) The fact that the *RM* of the integrated emission from the eastern component between 6 cm and 21 cm ($+38$ rad m^{-2}) differs from that appropriate to the radio source as a whole ($+68$ rad m^{-2}); and d) The discrepancy between each of the above mentioned values of *RM* and the range of values ($+42$ $-+62$ rad m^{-2}) inferred from Figure 4a, at the resolution of which the magnetic field commonly exhibits point to point coherence.

We have also determined the configuration of the magnetic field with the higher resolution of the 6 cm observations, by rotating each of the 6 cm electric vectors (Fig. 1b) by a constant angle, which was derived on the assumption that the *RM* is constant and equal to the mean of the values inferred from Figure 4a. Because the *RM* variation over the source is not large, this simplifying assumption will introduce negligible errors, of $\lesssim 3°$, in projected field direction. The resulting map of the magnetic field configuration is shown in Figure 6. The most striking feature of this diagram is that the field often runs parallel to the contours of total intensity, especially in the tail of the eastern component.

3. The 3C 386 Observations

The 6 cm total intensity and linear polarization maps are shown in Figure 7. They are the highest resolution maps yet presented of 3C 386. Earlier observations by

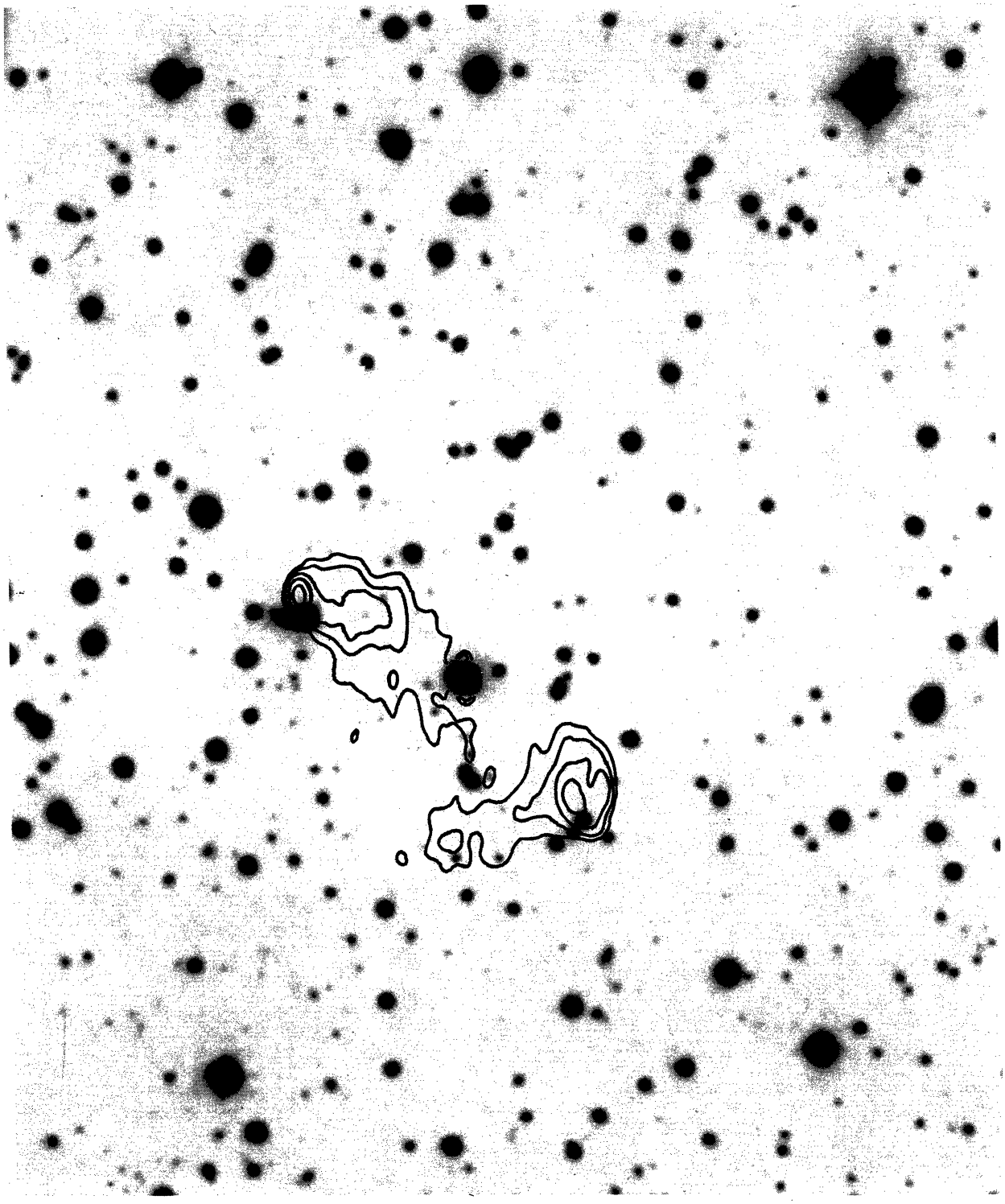

Fig. 3. Contours of the 6 cm total intensity of 3C 382 (Fig. 1a) superimposed on a copy of the Palomar Sky Survey red print (Copyright by the National Geographic Society—Palomar Sky Survey)

Becker and Kundu (1976) were undersampled and unable to present full structural details. The basic, roughly north-south, structure is that of an irregular double, although weaker emission lies to the east of the southern component ridge, and west of the northern one. The general pattern repeats at 21 cm (Fig. 8), the total intensity structure being very similar to that presented by Mackay (1970) with equivalent resolution.

The central component was detected by Becker and Kundu (1976) and their flux densities at 11 cm and

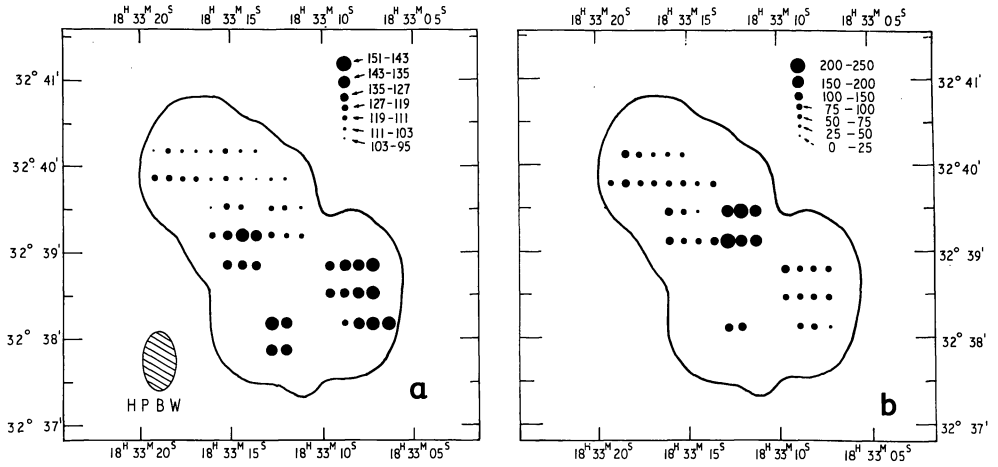

Fig. 4. Polarization properties obtained by comparing 6 cm and 21 cm maps of 3C 382 made with the same synthesized beam. **a** The difference between the measured position angles (in degrees). The values may be converted to the suggested rotation measure (see text) by multiplying by 0.42. **b** The depolarization ratio, defined as $100 \times$ (21 cm degree of polarization/6 cm degree of polarization)

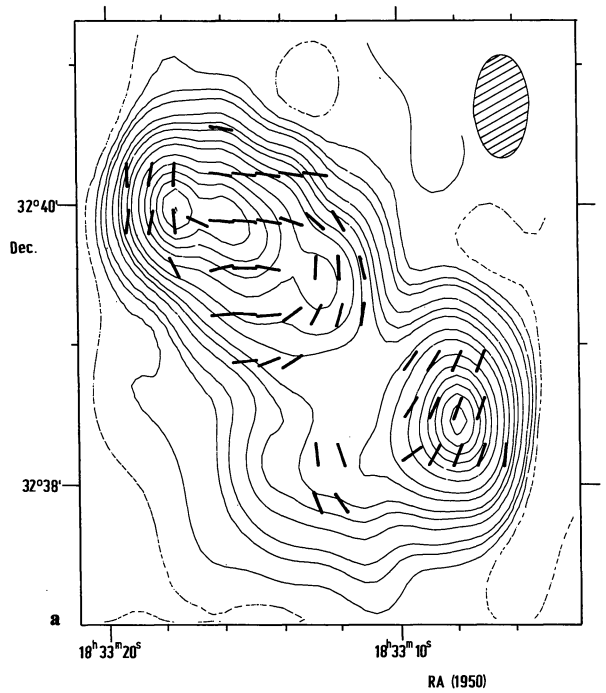

Fig. 5. Projected magnetic field with the 21 cm resolution, derived using rotation measure values from Fig. 4a

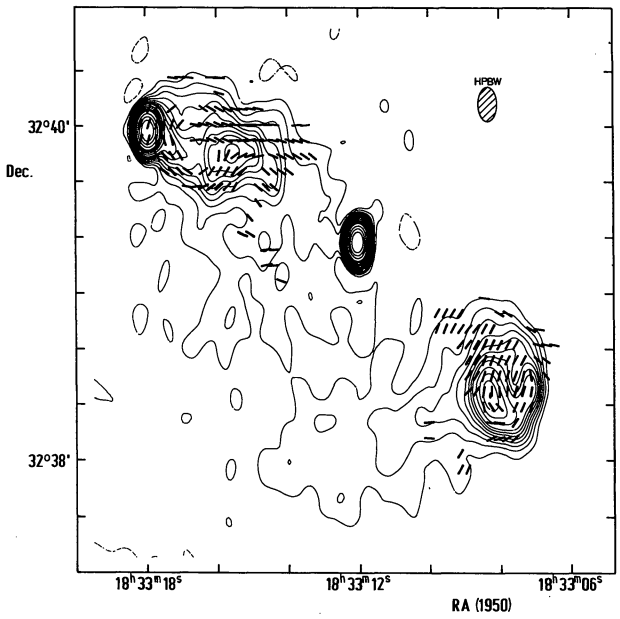

Fig. 6. Projected magnetic field direction, obtained by correcting the measured 6 cm position angles to zero wavelength using the suggested rotation measure (see text)

3.7 cm, when combined with our 6 cm value of 14 ± 2 mJy, give a spectral index, $\alpha = -0.7 \pm 0.2$. This component coincides with a 15^m galaxy (Fig. 9) which, as Becker and Kundu note, removes any doubt that 3C 386 is an extragalactic source (cf. Mackay, 1970). Earlier, Lynds (1971) made a convincing case for this interpretation when he showed that the redshift of the 3C 386 galaxy is, $z = 0.0177$.

Examination of the photograph used in Figure 9 suggests that the optical galaxy is slightly elliptical, with its minor axis parallel to the direction of the main radio ridge. The galaxy is listed in the Zwicky catalogue (Zwicky and Herzog, 1963), where it is classified as "extremely compact". There are no clusters of galaxies near 3C 386 though this might be partly due to absorption at this relatively low galactic latitude ($b = 10°.5$). Nevertheless, it seems unlikely that 3C 386 is a member of a cluster as 3C 382 appears to be.

Table 4 summarizes the observed radio properties of 3C 386 as derived from our data. There is little evi-

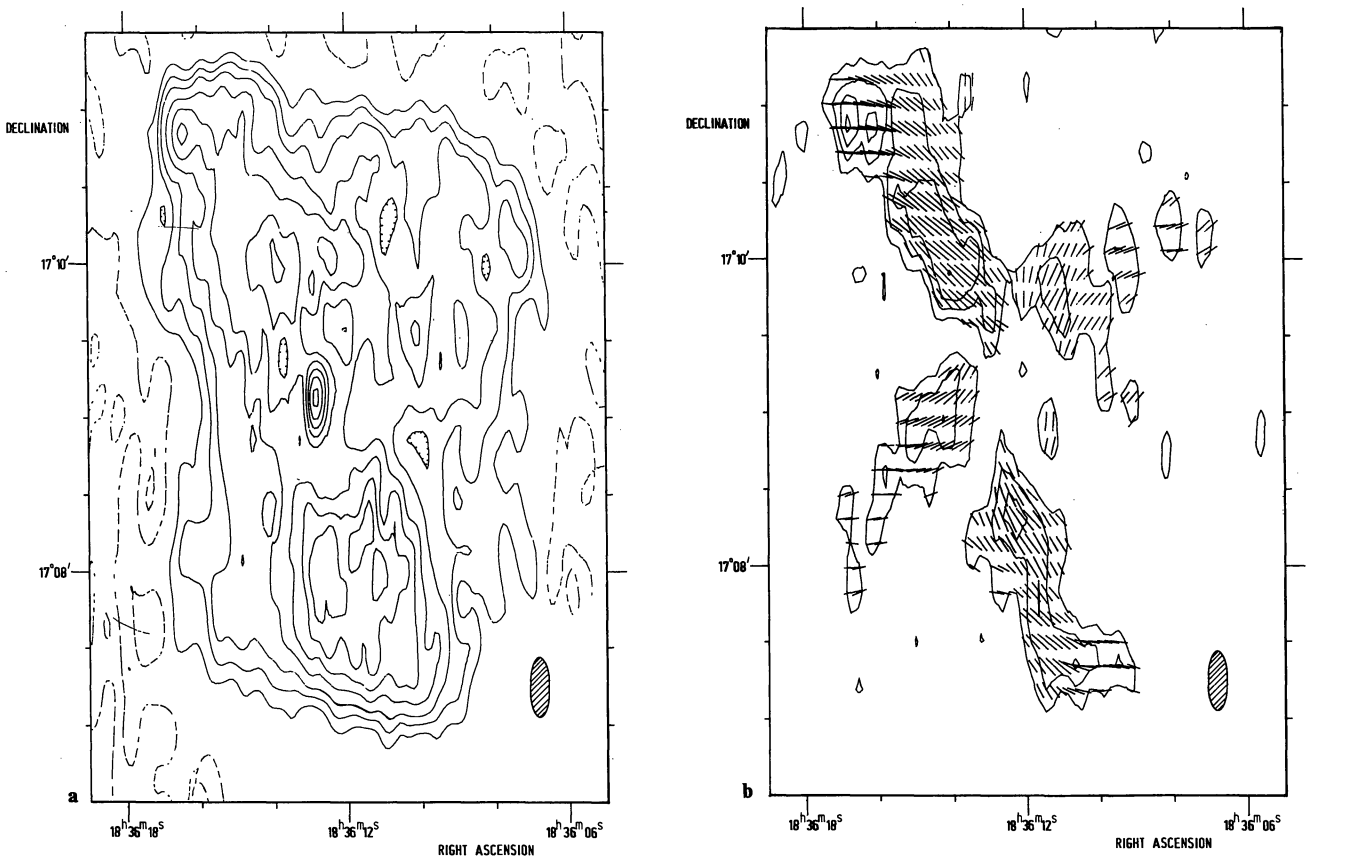

Fig. 7. Maps of 3C 386 at 6 cm. **a** The total intensity distribution. Contour values are −4, −2 (both dashed), 2, 4, 6, 9, 12, 15, 18, 21 and 24 mJy/beam. **b** Contours of linearly polarized intensity and the position angle of the electric vector (lines). Contour values are 2.5, 4, 5.5 and 7 mJy/beam. **c** Contours of the degree of linear polarization (values in per cent) superimposed on total intensity contours

dence for hot spots near the outer edges of the components, though some enhancement of the emission occurs in the northeastern corner (Fig. 7a). Much extended emission lies outside the two main components, and entirely surrounds the central source. Most of the structural detail, including the central component, is lost with the lower 21 cm resolution (Fig. 8a).

The maps of polarized intensity (Figs. 7b and 8b) not only show strong polarization in the two main components, but also a remarkable secondary ridge along position angle 150°, running through the plateau of extended emission. This secondary ridge is not apparent in the total intensity maps. As is clear from the 21 cm data (as well as the 6 cm data smoothed to the 21 cm resolution), the weaker emission is also polarized. The highest degree of polarization—30%–40% (with typical uncertainties of 10%) at 6 cm—is found in these faint, outlying regions.

Combining our integrated polarization position angles (Table 4) with other values (Gardner et al., 1969; Berge and Seielstad, 1967; Maltby and Seielstad, 1966) we obtain a mean RM of 74 rad m^{-2} for the source.

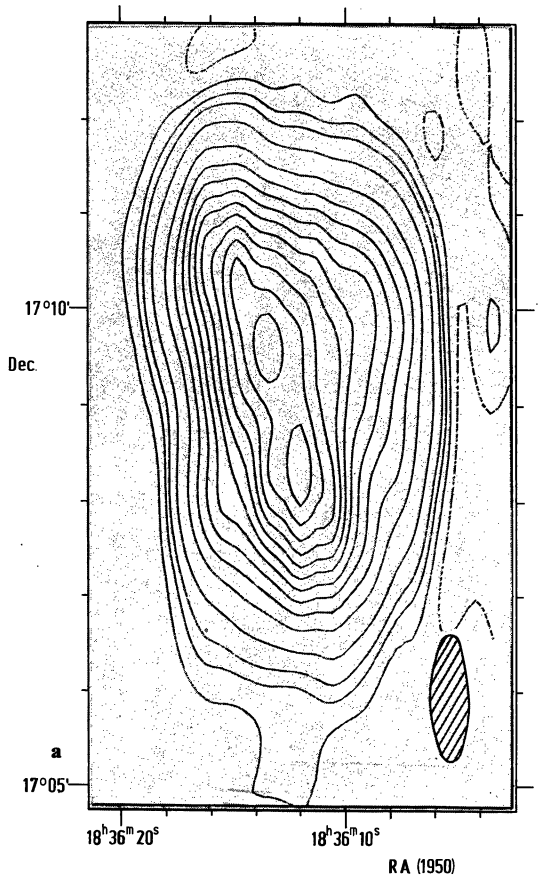

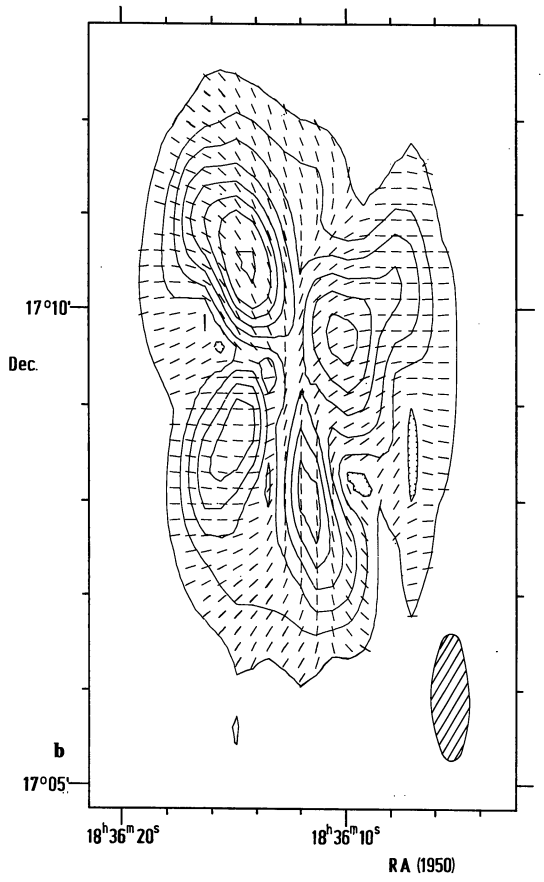

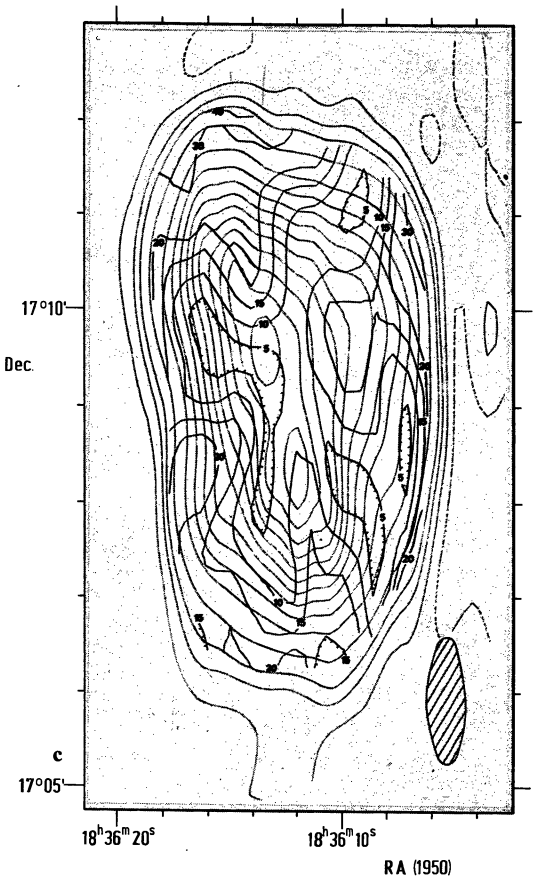

Fig. 8. Maps of 3C 386 made at 21 cm. **a** The total intensity shown with contours of −5 (dashed), 5, 15, 25, 50, 100, 150, 200, 250, 300, 350, 400, 450, 500 and 550 mJy/beam. **b** The linearly polarized intensity and position angle shown with contours of 5, 15, 25, 37.5, 50, 62.5, 75 and 100 mJy/beam. **c** Contours showing the percentage of linear polarization superimposed on a total intensity map

Table 4. Observed Radio Properties of 3 C 386

Angular size, major × minor axis	234″ × 88″
Position angle, major axis	20°
Flux density, 21 cm	7 Jy
Flux density, 6 cm	2.1 Jy
Spectral index, α_{21}^{6}	−1.0
Degree of polarization, 21 cm	1.1%
Polarization p.a., 21 cm	56°
Degree of polarization, 6 cm	4.1%
Polarization p.a., 6 cm	65°

Figure 10a shows the distribution of the difference in position angles, as derived from our 6 cm and 21 cm data (the differences are readily converted to *RM* values), while 10b compares the degree of polarization at the two wavelengths. Although there is no clear pattern in the latter diagram, the *RM* shows a gradual increase as one proceeds northwards along the source, with an overall change of about 20 rad m^{-2}.

In Figure 11, the individual values of *RM* over the source (Fig. 10a) have been used to construct a map of the projected magnetic field direction with the resolution

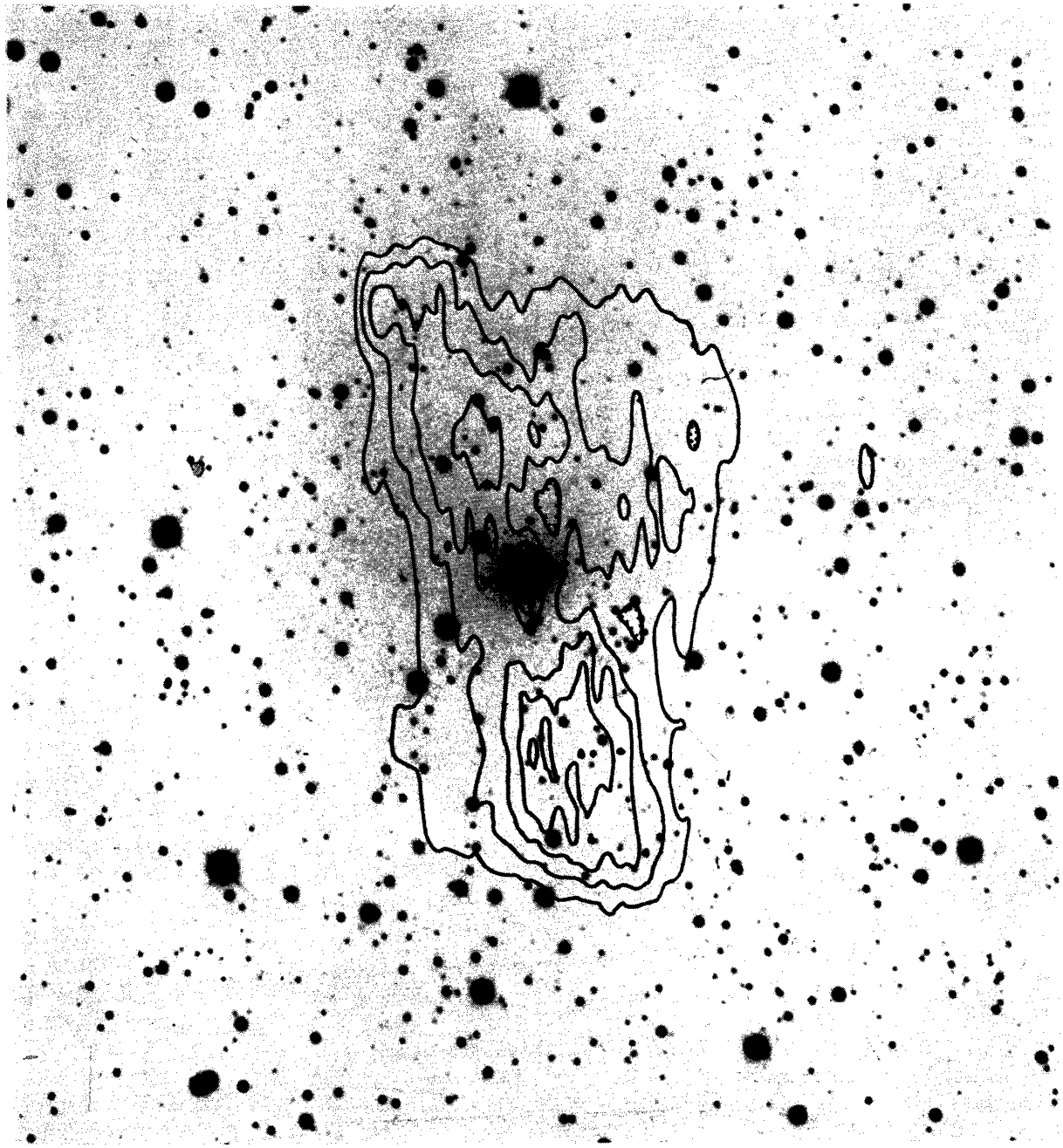

Fig. 9. The 6 cm map of 3C 386 superimposed on a Lick 120-inch reflector red photograph obtained by H. Spinrad

of the 21 cm observations. Using the average *RM* from Fig. 10a and the 6 cm position angles (Fig. 7b), a map of the magnetic field directions at the higher resolution of the 6 cm map has also been derived (cf. Section 2) and is shown in Figure 12. Both Figures 11 and 12 reveal that the field runs in a largely circumferential sense about the center of the source.

4. Discussion and Conclusions

Derived physical parameters for the two sources are summarized in Table 5. The values obtained are similar to those presented by Riley and Branson (1973) and Becker and Kundu (1976). The most interesting new results of the present observations involve polarization properties, so our discussion will especially focus on this aspect.

First let us consider variations in the *RM*. Figures 4a and 10a show clearly that for both objects the *RM* is not uniform over the source; variations of the *RM* over the individual components as well as differences between the components are found. It is unlikely that these variations reflect changes in the contribution of

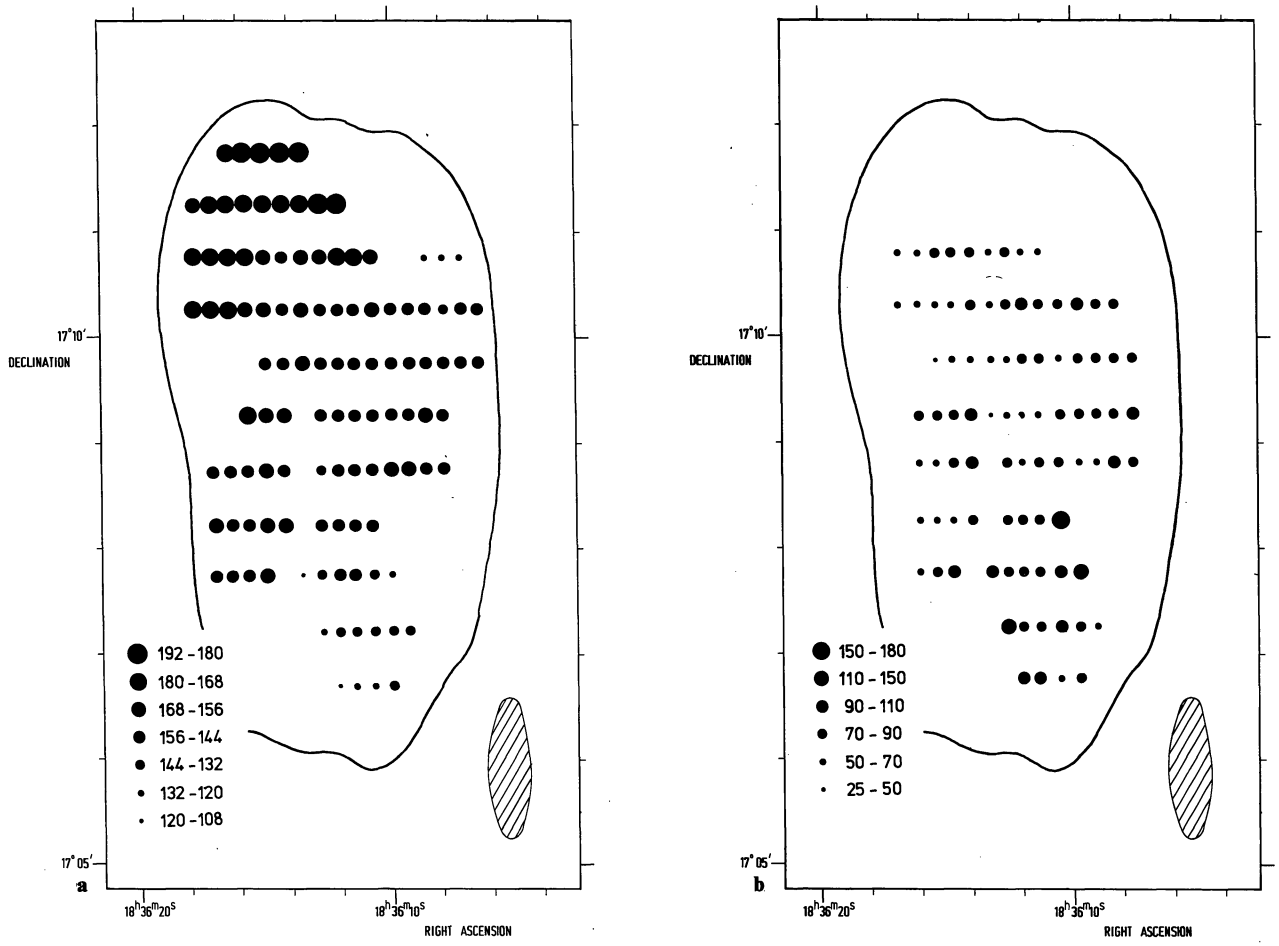

Fig. 10. Polarization properties of 3C 386, obtained by comparing 6 cm and 21 cm maps made with the same resolution. **a** The difference between the measured position angles (in degrees). These values can be converted to the rotation measure discussed in the text by multiplying by 0.42. **b** The depolarization ratio, 100 × (21 cm degree of polarization/6 cm degree of polarization)

our Galaxy to the *RM*—for example, sources larger than 1′ do not show any tendency to depolarize more rapidly than compact sources (Strom, 1973). However, in general, the observed *RM* will contain a uniform component as well, to which the galaxy probably makes a significant contribution.

To address the question of whether the changes in *RM* across each source might be intrinsic, we may try to correlate them with some other source property. The *RM* depends on the (integrated) product of electron density and the uniform component of the magnetic field strength: $RM \propto n_e LB \cos\theta$, where n_e and B are considered to be uniformly distributed along a path-length L, and θ is the angle between the field direction and the line of sight. n_e and L are not uniquely related to other measurable radio properties. The radio brightness depends on the total magnetic field strength, while it is the uniform component which dominates the *RM*. Since the degree of disorder in the field may well be correlated with changes in brightness, the relationship between such changes and variations in *RM* is unlikely to be simple. This does suggest, however, that in our investigation, regions with large changes in brightness should be avoided.

The remaining parameter, θ, is more promising. Changes in the field direction will, in general, cause changes both in the magnitude of the field component along the line of sight (and hence in the *RM*) and in the direction of the component in the plane of the sky. We might, therefore, expect a relation between *RM* and the position angle of the field in the plane of the sky, ψ. If the magnitudes of n_e, B and L remain constant then, approximately, $\Delta RM \propto \Delta\psi$ in a wide variety of physical situations.

In Figure 13a position angles from Figure 5 are plotted against the corresponding values of *RM* for the brightest part of the southwest component of 3C 382. To obtain roughly one point per beam alternate values have been taken from the diagram. Over this portion of the component there are no large changes in brightness. A least squares fit to the data is also shown whose coefficient of determination is, $r^2 = 0.8$.

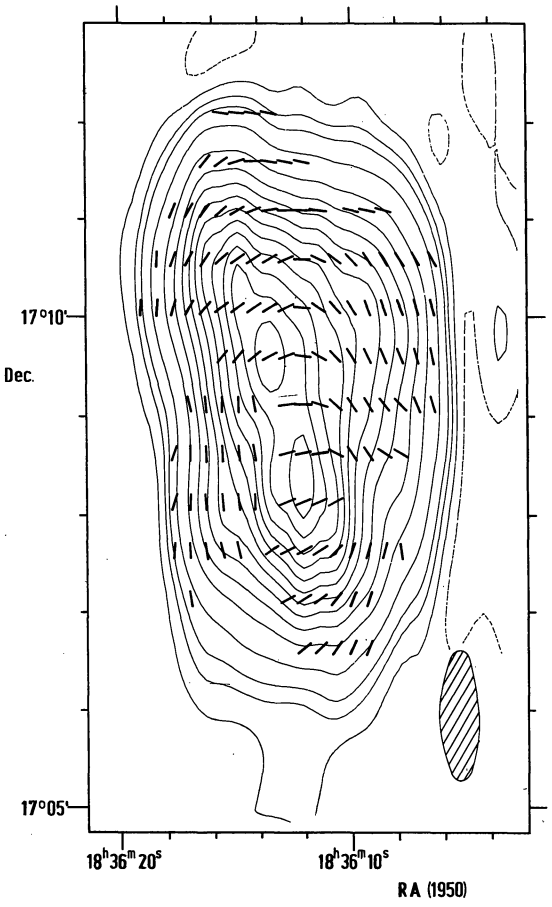

Fig. 11. Projected magnetic field for 3C 386 derived from the rotation measure values in Fig. 10a

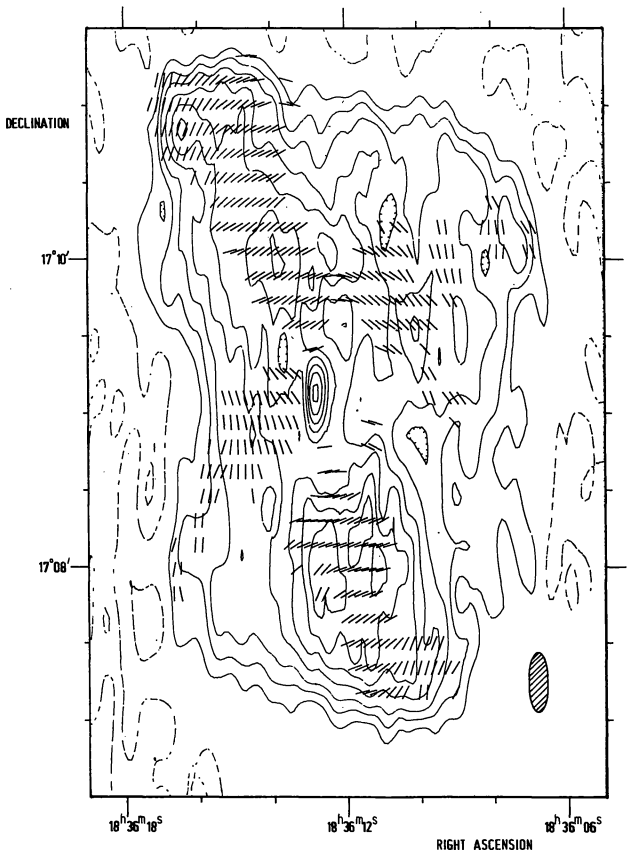

Fig. 12. Projected magnetic field direction obtained by correcting the 6 cm position angles to zero wavelength using the integrated rotation measure (see text)

For 3C 386 a section through the northern component has been taken, corresponding to the fourth and fifth rows of position angles from the top in Figure 11. In this area, the polarization is strong, there are no large variations in radio brightness and there is a smooth change in position angle from one side to the other. The relationship between *RM* and position angle is shown in Figure 13b, together with a least squares fit to the data ($r^2 = 0.8$).

The evidence in Figure 13 clearly favors a linear correlation between *RM* and intrinsic field direction. Some caution must, however, be exercised before jumping to the conclusion that we have proven a causal relationship between the two. The chance superposition of a foreground gradient in the *RM* could, in some circumstances, give rise to a similar correlation. There is, however, evidence for a similar relationship in 3C 123 (Kronberg and Strom, 1977) where the magnitude of the change in *RM* makes a foreground gradient highly unlikely. In view of this we tentatively conclude that the observed changes in *RM* originate within the radio emitting regions.

Table 5. Derived Physical Parameters

z	3C 382 0.0578	3C 386 0.017
Luminosity Distance[a] (Mpc)	234	68
Overall linear size (kpc)	187	75
P_{21} (W Hz^{-1})	$2.1\ 10^{25}$ (east) $1.4\ 10^{25}$ (west) $3.6\ 10^{25}$ (total)	$3.9\ 10^{24}$
Luminosity[b] (erg s^{-1})	$1.6\ 10^{42}$ (east) $1.1\ 10^{42}$ (west) $2.6\ 10^{42}$ (total)	$2.8\ 10^{41}$
Equipartition magnetic field[c] (G)	$8\ 10^{-6}$ (east) $7.6\ 10^{-6}$ (west) $7.8\ 10^{-6}$ (average)	$6.2\ 10^{-6}$
Total equipartition energy[c] (erg)	$1.3\ 10^{58}$ (east) $1.0\ 10^{58}$ (west) $2.3\ 10^{58}$ (total)	$3.4\ 10^{57}$

[a] Estimates of physical parameters have assumed a Hubble constant $H_0 = 75$ km s^{-1} Mpc^{-1} and an Einstein—de Sitter cosmology

[b] Over the range 10 MHz to 10 GHz

[c] Assuming equal energy densities of relativistic electrons and heavy particles

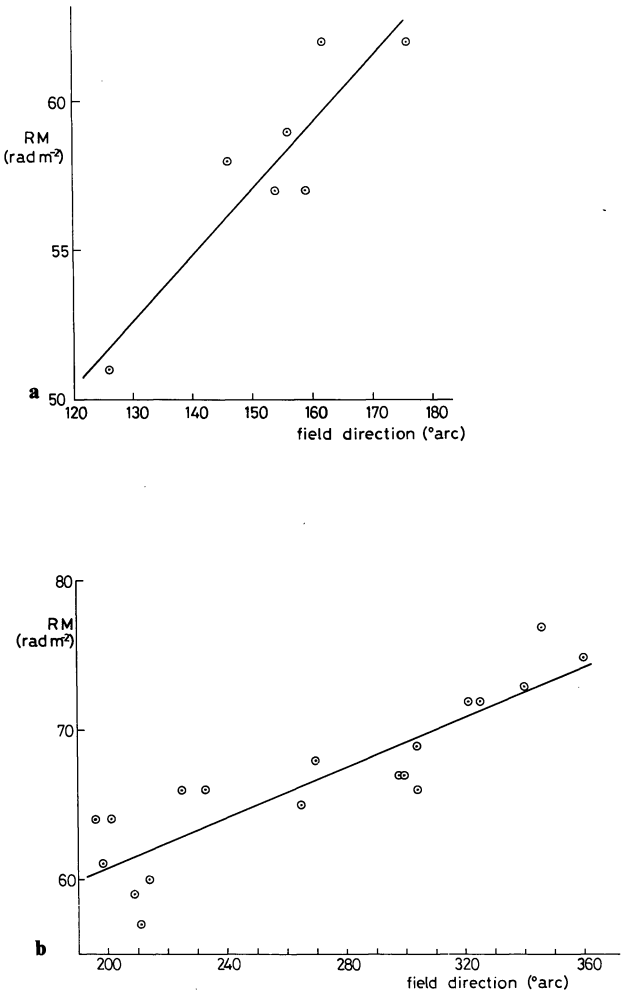

Fig. 13. Correlation between intrinsic magnetic field direction and rotation measure (see text). **a** The southwestern component of 3C 382. **b** Part of the northern component of 3C 386

A more detailed comparison based on each source in its entirety is difficult, partly because the magnetic field structures are generally complex. One feature does recur in several places: a circumferential alignment of the magnetic field direction. We have already pointed out that this is apparent in the overall field structure for 3C 386 (Figs. 11 and 12). Such an arrangement can also be seen in 3C 382 (Fig. 6) behind the bright hot spot in the northeast component, and in the brightest part of the southwest one. The fact that it occurs where broad emission regions have a near circular symmetry suggests a magnetic field being swept along and compressed by outwardly expanding material, thereby acquiring alignment perpendicular to the expansion direction (see also Fomalont, 1972).

A curious feature of 3C 386 is the two "arms" of polarized emission which extend northwest and southeast of the center (Figs. 7b and 8b). Their existence, which is not hinted at by the largely featureless total intensity emission in this region, presumably indicates areas where the magnetic field is well ordered, although there has been no concomitant enhancement of the volume emissivity as there is along the main radio ridge. The two sets of polarized components suggest that material may have been expelled in more than one direction from the central galaxy. The fact that the radio emission encircles the central source may also imply that the various outbursts have not been collinear.

A very different origin seems likely for the deviations from simple symmetry we observe in 3C 382. The distortions in the southwest component have already been noted. A related phenomenon appears to be the large area of very weak emission south of the northeast and central components. Both suggest that either the galaxy is moving in a northerly direction or intergalactic material is blowing south past it. The latter possibility might imply that material is still falling towards the center of the cluster Zw 1831.2+3154, since 3C 382 lies near its northern edge. The angle which the low brightness "tail" of the southwest component makes with the source major axis suggests that the gas is moving past 3C 382 at a rate comparable to the speed of the component away from the optical galaxy.

Osterbrock et al. (1976) have noted that the extremely broad emission lines of 3C 382 imply that its optical spectrum is very similar to that of a type I Seyfert. This and the radio variability of its central component indicate continued nuclear activity. Since at least 15 type I Seyfert galaxies are associated with X-ray sources (Elvis et al., 1978), it is interesting to consider whether 3C 382 may also be an X-ray emitter. Elvis et al. (1978) list 3C 382 as a marginal ($3\sigma-5\sigma$) detection in their survey of Seyferts with the Ariel V Sky Survey Instrument. The X-ray source 4U 1825+33 (Forman et al., 1977) is also a possible counterpart of 3C 382. Although 3C 382 falls outside the error box of this source, there are several reasons for believing that the two may nevertheless be related: The 4U error box is very elongated and the position determined in the narrow dimension agrees well with that of 3C 382; 4U 1825+33 is listed as possibly confused so it "...was not a unique choice based upon the available lines of position"; Since the X-radiation probably originates in the compact nucleus it may, like the X-ray emission from some other Seyferts and the radio emission from 3C 382 itself, be variable which would increase the X-ray position uncertainty. If 4U 1825+33 and 3C 382 are associated, then the X-ray luminosity is about $3\ 10^{44}$ erg s^{-1}, which is comparable with the X-ray luminosities of NGC 1275, 3C 120 and 3C 390.3.

We wish to thank Dr. H. Spinrad for providing the photograph of the 3C 386 galaxy used in Figure 9, and Dr. J. R. Baker for communicating data in advance of publication. During the course of this work, ASW has been supported by Royal Society European Program and Science Research Council Fellowships. The Westerbork Synthesis Radio Telescope is operated by the

Netherlands Foundation for Radio Astronomy with financial support from the Netherlands Organization for the Advancement of Pure Research (Z. W. O.).

References

Adams, T. F.: 1977, *Astrophys. J. Suppl.* **33**, 19
Becker, R. H., Kundu, M. R.: 1976, *Astrophys. J.* **207**, 29
Berge, G. L., Seielstad, G. A.: 1967, *Astrophys. J.* **148**, 367
Conway, R. G., Gilbert, J. A., Kronberg, P. P., Strom, R. G.: 1972, *Monthly Notices Roy. Astron. Soc.* **157**, 443
Elvis, M., Maccacaro, T., Wilson, A. S., Ward, M. J., Penston, M. V., Fosbury, R. A. E., Perola, G. C.: 1978, *Monthly Notices Roy. Astron. Soc.* **183**, 129
Fanaroff, B. L., Riley, J. M.: 1974, *Monthly Notices Roy. Astron. Soc.* **167**, 31P
Fomalont, E. B.: 1972, *Astrophys. Letters* **12**, 187
Forman, W., Jones, C., Cominsky, L., Julien, P., Murray, S., Peters, G., Tananbaum, H., Giacconi, R.: 1977, Center for Astrophysics, Preprint Series No. 763
Gardner, F. F., Morris, D., Whiteoak, J. B.: 1969, *Australian J. Phys.* **22**, 79
Gavazzi, G., Perola, G. C.: 1977, preprint
Harris, A.: 1974, *Monthly Notices Roy. Astron. Soc.* **166**, 449
Högbom, J. A., Brouw, W. N.: 1974, *Astron. Astrophys.* **33**, 289
Högbom, J. A.: 1974, *Astron. Astrophys. Suppl.* **15**, 417
Kronberg, P. P., Strom, R. G.: 1977, *Astrophys. J.* **215**, 438
Lynds, R.: 1971, *Astrophys. J. Letters* **168**, L87
Macdonald, G. H., Kenderdine, S., Neville, A. C.: 1968, *Monthly Notices Roy. Astron. Soc.* **138**, 259
Mackay, C. D.: 1970, *Astrophys. Letters* **5**, 173
Maltby, P., Seielstad, G. A.: 1966, *Astrophys. J.* **144**, 216
Osterbrock, D. E., Koski, A. T., Phillips, M. M.: 1976, *Astrophys. J.* **206**, 898
Riley, J. M., Branson, N. J. B. A.: 1973, *Monthly Notices Roy. Astron. Soc.* **164**, 271
Schmidt, M.: 1965, *Astrophys. J.* **141**, 1
Someren Gréve, H. W. van: 1974, *Astron. Astrophys. Suppl.* **15**, 343
Strom, R. G.: 1973, *Astron. Astrophys.* **25**, 303
Weiler, K. W.: 1973, *Astron. Astrophys.* **26**, 403
Zwicky, F., Herzog, E.: 1963, Catalogue of Galaxies and Clusters of Galaxies, Vol. II. California Institute of Technology